Cancer Microenvironment manuscript No.
(will be inserted by the editor)

Cross-talk between circRNAs and mRNAs modulates miRNA-mediated circuits and affects melanoma plasticity

Maria Rita Fumagalli · Maria Chiara Lionetti · Stefano Zapperi · Caterina A.M. La Porta

Received: date / Accepted: date

Abstract CircularRNAs (circRNAs) are non-coding RNAs which compete for microRNA (miRNA) binding, influencing the abundance and stability of other RNA species. Herein we have investigated the effect of circRNAs on the mir200-ZEB1 feedback loop during phenotypic switching of human melanoma cells. To this end, we quantify the expression level of the ZEB1 circuit in four primary and metastatic human melanoma cell lines and compare the results with data from public repositories for human melanoma and breast cancer, showing similarities between different tumor types. Our findings show a strong correlation between the level of expression of ZEB1 and aggressiveness of melanoma and breast tumors. Interestingly, analyzing human melanoma cell IgR39 during phenotypic switching, we observe changes in the expression of ZEB1 while circZEB does not change. To understand these experimental observations, we propose a mathematical model of the mir200-ZEB1 circuit including interactions with circRNA. According to the model, a constant high expression of circZEB1 during phenotypic switching suggests the presence of a back-splicing factor limiting circRNA production. Taken together, our results suggest a possible use of circZEB1 as a biomarker of aggressiveness in melanoma.

Keywords circRNA · ZEB1 · melanoma · phenotypic switching

1 Introduction

Cancer plasticity is an emerging property of tumor cells that is leading us to reconsider the classical strategies for therapeutic intervention [1,2,3,4,5]. Recently, our group showed that human melanoma cells dynamically change their phenotype by expressing epithelial to mesenchymal transition (EMT) markers, in a way that is regulated by complex network of miRNAs [6]. This plasticity allows cells to either grow or stop growing in order to maintain a specific proportion of EMT-marker expressing cells in the bulk [6]. The EMT is one the key processes that cells undergo in order to gain a migratory phenotype and it is thus relevant for metastasis

Noncoding RNAs, such as microRNAs and circular RNAs (circRNAs) are all recognized to play a key regulatory role in physiological and pathological cellular processes [7]. In this respect, circRNAs, single-strand endogenous noncoding RNA closed in a loop [8], are widely expressed in mammalian cells and differential expressed in various tissues and pathological conditions[9,10,11,8,7]. Thanks to their circular form, circRNAs are more stable than linear RNAs and since they have been detected in exosomes and in the blood, they appear to be ideal candidates to act as biomarkers [12,13,14,15,16]. In this connection, it has been recently demonstrated that circRNAs partecipate to the complex post-transcriptional regulatory network, competing

M. R. Fumagalli
Consiglio Nazionale delle Ricerche, Istituto di Biofisica, via Celoria 26, 20133 Milano, Italy
Center for Complexity and Biosystems, Department of Environmental Science and Policy, University of Milan, via Celoria 26, 20133 Milano, Italy

M. C. Lionetti
Center for Complexity and Biosystems, Department of Environmental Science and Policy, University of Milan, via Celoria 26, 20133 Milano, Italy

S. Zapperi
Center for Complexity and Biosystems, Department of Physics, University of Milano, via Celoria 16, 20133 Milano, Italy
CNR - Consiglio Nazionale delle Ricerche, Istituto di Chimica della Materia Condensata e di Tecnologie per l'Energia, Via R. Cozzi 53, 20125 Milano, Italy

C. A. M. La Porta
Center for Complexity and Biosystems, Department of Environmental Science and Policy, University of Milan, via Celoria 26, 20133 Milano, Italy
Consiglio Nazionale delle Ricerche, Istituto di Biofisica, via Celoria 26, 20133 Milano, Italy.
Corresponding author:E-mail: caterina.laporta@unimi.it

with mRNAs for microRNA binding and affecting the abundance and stability of other RNA species [9,17,18, 7,19].

This competition affects the abundance and stability of other RNAs [19]. The existence of different miRNA targets which have the same binding sites, leads to an indirect, miRNA-mediated, cross-talk between competitive endogenous RNAs (ceRNA) [20,21,22].

In the present study, we investigated the possible regulative role of circRNAs in a ceRNA circuit involved in the EMT by combining experiments, computational models and data analysis. The core of the EMT process is the double negative feed-back loop that includes ZEB1 and members of mir200 family and SNAIL1 as external transcriptional activator [23,24,25]. The human gene ZEB1 can produce multiple functional RNAs including circRNAs [26,27,28,29]. One of them, circ-ZEB1.33 [29] (circZEB1), is the product of backsplicing of exons 2 to 4 of ZEB1 transcript variant 1 (NM 001128128[28,29] and contains a binding site for hsa-mir200a-3p and hsa-mir141-3p, both belonging to mir200 family [28]. The latter is a well-known post-transcriptional regulators of ZEB1 [23,30,31,32,33]. First, we compared, herein, the level of expression of members of ZEB1 circuit in human primary and metastatic melanoma cells derived from the same patient (WM115/WM266 and IgR39/IgR37 cells, primary and metastatic, respectively). Then, we investigated the dynamic changes of this ZEB circuit during phenotypic switching in human melanoma IgR39 cells [6]. We also checked the level of expression of ZEB1 in samples of primary and metastatic patients stored on public repositories to confirm our experimental results. Finally, to evaluate if our results were specific for melanoma only, we analyzed the level of expression of ZEB1 in primary and metastatic breast cancer.

All together our results show that circZEB1 is a biomarker of aggressiveness for melanoma.

2 Materials and methods

2.1 Cell culture

IgR39 and IgR37 cells (primary and metastatic human melanoma cells, respectively) were obtained from Deutsche Sammlung von Mikroorganismen und Zellkulturen GmbH [6] and WM115 and WM266 (primary and metastatic human melanoma cells, respectively) from ATCC (CRL 1675, CRL 1676, respectively) [34]. All cell lines were cultured in DMEM, 15% FBS supplemented with 1% MEM vitamin, 1% MEM aminoacid, 1% antibiotics (Penicillin/Streptomycin), 1% L-glutamine (complete medium) at 37°C in a 5% CO2 humidified environment.

2.2 Flow cyometry

Cells are sorted for phycoerythrin (PE) anti-human CXCR6 (code:FAB699P-025, R& D System, USA). For each flow cytometry evaluation, a minimum of $4 \cdot 10^7$ cells were stained and at least $5 \cdot 10^5$ events were collected and analyzed. Flow cytometry sorting and analysis was performed using a FACSAria flow cytometer (Becton, Dickinson and Company, BD, Mountain View, CA). Data were analyzed using FlowJo software (Tree Star, Inc., San Carlos, CA).

2.3 qRT-PCR

SNAI1, ZEB1, circZEB1 and GAPDH specific primers were designed using the primer analysis software Primer3[35] and aligned on human genomic transcripts using Blast [36] in order to minimize off-target effects. Divergent primers encompassing backsplicing site were designed for CircZEB1 based on fasta sequenc of hsa_circ_0004907 obtained from CircBase[29]. Primers for ZEB1 mRNA were designed on exon 7 of transcript ENST00000446923 (RefSeq NM_001128128) that is in shared by 7 of the 9 protein coding transcripts according to Ensembl database (last accessed March 2019[27]). The following primers were selected:
CircZEB1_F CCAGAAGCCAGTGGTCATGA, CircZEB1_R GTCATCCTCCCAGCAGTTCT,
ZEB1_F GAGAAGCCATATGAATGCCCA, ZEB1_R GTATCTGTGGTCGTGTGGGA,
SNAI1_F TACAGGACAAAGGCTGACAGA, SNAI1_R CGGGGCATCTCAGACTCTAG,
GAPDH_F CACATCGCTCAGACACCATG, GAPDH_R TGACGGTGCCATGGAATTTG.
Briefly, total RNA was extracted with the Guanidinium Thiocyanate-Phenol-Chloroform extraction with 1 ml of TRIzol Reagent. RNA samples were incubated for 5 minutes at room temperature. After adding 0.2 ml of chloroform in each sample, the tube was vigorously shaked and centrifuged at $12 \cdot 10^3$ x g for 15 minutes at 4°C. The aqueous phase obtained was collected and placed into a new tube and 0.5 mL of 100% isopropanol was added. After 10 minutes at room temperature samples were centrifuged at $12 \cdot 10^3$ x g for 10 minutes at 4°C.

The supernatant has been removed from the tube and the pellet washed with 1 ml of 75% ethanol, vortexed briefly and centrifuged. RNA pellet has been left air drying and resuspended in 20 μl of RNAse-free water. RNA concentration and purity was determined by using Nanodrop (Eppendorf).

Synthesis of cDNA was performed on 1 μg of total RNA reverse transcribed (RT) using Vilo IV Superscript cDNA synthesis kit (Invitrogen, CA) according to manufacturer's instructions. Real time q-RT-PCR analysis was performed using ViiA7 Real Time PCR system (Applied Biosystems). Each primer pair was tested at least in six replicates using 25ng of cDNA. The PCR-reaction included 25ng of template cDNA, 5 μM of each (forward and reverse) primers, 2 μl of RNAse-free water and 10 μl of LUNA Universal SYBR Green Mastermix (New England Biosystems), in a total volume of 20 μl. Cycling conditions were as follows: 95°C enzyme activation for 10 min, followed by 50 cycles of amplification: 15" at 95°C for denaturing, 1 min at 60°C for annealing/elongation. Quantified values were normalized against the input determined by the housekeeping human gene GAPDH. Average ΔCt was calculated for each plate and averaged over replicated plates and plotted as $2^{-\Delta Ct}$ using R[37].

2.4 GDC expression data

Gene expression levels in primary and metastatic tumor samples from patients were obtained from Genomic Data Commons (GDC) data portal [38] RNA-seq data. A total of 468 transcriptome profile from 465 cases classified as melanoma (primary site skin) including 103 primary tumors and 366 metastatic ones were obtained. Among these only two samples were classified as primary and metastatic tumors form the same patient (TCGA-ER-A2NF), and two samples were originated from normal solid tissue and metastatic tumor of a patient (TCGA-GN-A4U8). Regarding breast cancer, 1189 transcriptome profiles were obtained from GDC database for cases that have primary site in breast tissue. Seven of these samples were metastatic and transcriptome of all the corresponding primary tumors were retrieved. Samples annotated by GDC as treated with neoadjuvant therapy or not meeting the study protocol were excluded. ZEB1 expression was estimated using the number of aligned fragments per kilobase of transcript per million reads (FPKM) and was normalized using GAPDH as housekeeping. Note that comparing the relative expression of ZEB1 instead of absolute values allows to eliminate bias due to the normalization procedure used to obtain expression values. Moreover, we considered as additional housekeeping ribosomal protein L19 (RPL19) and PGK2 to verify that the choice of GAPDH does not influence the obtained results (data not shown).

2.5 Mathematical Model of ZEB1 circuit

MiRNA-mediated interactions are modeled using a set of differential equations following our previous work [19], details of the model are presented in the Supplementary information. Briefly, our model comprises two kinds of post-transcriptional regulation (the binding of mRNA (T) and circRNA (C) by miRNA (μ) and circRNA creation) and two possible transcriptional regulations (promoter silencing and enhancing) (Fig.3a,c). In general, all these interactions but circRNA creation can involve more than two molecules with multiple binding and partial or reinforced effects (cooperativity of the binding). In accordance with biological evidences, since our aim is to reproduce ZEB1-mir200a circuit, we consider two non competing equivalent biding sites for mir200a on ZEB1 3'UTR and one on circZEB1 [39]. SNAI1 and ZEB1 repression/activation on mir200/ZEB1 promoter was modeled using appropriate Hill functions (see. Suppl.Materials, [40,41]). We do not model explicitly SNAI1 production/degradation considering it as a tunable external input (see Fig.3c).

Decay rate were set according to experimental estimate as follows. MiRNA half life, experimentally estimated to range from $\approx$ 8 hours up to days, was set to $\gamma_\mu = 0.001 min^{-1}$ while mRNA half life is typically of few hours [42,43,44] and was set to $\gamma_T = 0.01 min^{-1}$. Since circRNA are much more stable than mRNAs, with typical half life of the order of days, closer to miRNA values [10], we set its decay rate $\gamma_C = \gamma_\mu = 0.001 min^{-1}$. Protein decay rate was set to $0.01 min^{-1}$ corresponding to estimated ZEB1 half life ($\approx 2h$ [40]). For production and interaction rates, we refer to former works and experimentally estimated rates [21,45,40,19].We treated the contributions of the other species as a constant and implicitly including them into the decay rates.

Numerical solutions of equations at steady state and Gillespie simulations were performed using Mathematica v.10 and python Stochpy library. Plots were created using Python [46] and R [37].

3 Results

3.1 Expression of ZEB1 circuit in primary and metastatic human melanoma cells

The level of expression of ZEB1, a key regulator of EMT [23,24,25], is modulated by the external transcription factor SNAI1 and by mir200 family (Fig. 1).

We first checked by qRT-PCR the level of expression of the mRNAs ZEB1, circZEB and SNAI1 in two different melanoma cell lines obtained from two patients at different stage of aggressiveness, primary or metastatic (Fig. 2). In both cells, we observed a decreased level of expression of SNAI1, ZEB1 and circZEB1 in metastatic cells (Fig. 2).The magnitude of this decrease is, however, dependent by the cell line, possibly representing the specific biological characteristics of each patient.

To confirm that our results were not depending on in vitro cell condition, we analyzed the level of expression of ZEB1 for data stored in public repositories (GDC database) obtained from tumors classified as primary and metastatic melanoma derived from the same patient. [38]. As shown in Fig. 3, we confirmed the decreased level of expression in metastatic samples of ZEB1. To investigate if this decrease was melanoma specific, we analyzed the level of expression of ZEB1 in breast cancer (primary and metastasis) using again public repositories (GDC database). Fig. 3 clearly shows that the level of expression of ZEB1 is lower in the metastatic samples with respect to the primary tumors.

3.2 Constant expression of circZEB1 during phenotipic switching

We sorted negative IgR39 cells for CSC markers and we measured the level of expression of the circuit of ZEB1 by qRT-PCR at different times: ten (T10) and twenty days (T20) after sorting, respectively.. As shown in our previous paper, CSC markers are dynamically expressed with a switch on of EMT-related genes at T3, followed by an expansion of the CSC population until T10 and finally the switch off of EMT genes and a return to stady-state conditions at T20 [6]. As shown in Fig. 4, we observed a significant increase of mRNAs ZEB1 and SNAI1 at the CSC overshoot (T10) and a decrease at T20 towards the steady state (Fig. 4). On the other hand, we consistently found high and relatively constant level of circZEB1 at the overshoot and at T20 (Fig. 4).

3.3 Mathematical model for miRNA-mediated ceRNA circuit

*Steady state solution of the model.*MiRNA-mediated interactions were modeled using a set of differential equations in agreement with our previous work [19] and as described in detail in Material Methods and Supplementary information. We consider two kinds of ceRNA circuits: a more general case with one miRNA (μ) regulating two targets (mRNA, T and circRNA C) without a transcription regulation layer (Fig. 5a) and the specific case of ZEB1-mir200a network comprising transcriptional silencing of the miRNA, self-activation of the target and external transcriptional regulation (input, Fig. 5c). The introduction of self-activation and transcriptional silencing of the miRNA dramatically changes the phenomenology of the model, leading to the possibility of multistable regions (Fig. S1b,d, see also Suppl. information). In our model, the mRNA transcription rate can vary in a limited range of values when we consider the circuit in (Fig. 5c), while is theoretically unlimited for the more general circuit (Fig. 5a). According to our model, at equilibrium the free mRNA (T_{eq}) and circRNA (C_{eq}) concentrations are given by

$$\begin{aligned} T_{eq} &= \frac{\kappa_T}{\gamma_T(1+\mu_{eq}/\mu_T)} \\ C_{eq} &= \frac{K_C(T)}{\gamma_C(1+\mu_{eq}/\mu_C} \end{aligned} \tag{1}$$

where κ and γ are the production and decay rates, μ_{eq} is the amount of free miRNA molecules while μ_T and μ_C represent the thresholds determining if C and T are highly influenced by miRNA presence (i.e. when $\mu \gg \mu_i$, bound state) or are almost free (i.e. when $\mu \ll \mu_i$). These thresholds are directly proportional to the decay rate γ_i and inversely proportional to the miRNA-ceRNA affinity. Thus,for a given set of parameters, species with longer half-life and higher miRNA affinity are much more influenced by miRNA, while fast-decaying or low affinity species are less sensitive to variations in miRNA concentration.

The solution reported in Eq. 1 shows that T_{eq} and C_{eq} are coupled by two factors: the presence of mu_{eq} at denominator and the circRNA production rate K_C.

*Linear dependence of circRNA on mRNA concentration.*The simplest non-trivial case that can be considered for circRNA production rate is a direct proportionality between K_C and the abundance of the associated mRNA (i.e. $K_C(T) = \epsilon T$). This assumption implies that a constant fraction of the total RNA produced is in the form of cirRNA. In this case, it is immediate to verify that circRNA grows faster than linearly with T due to miRNA coupling, until the contribution of miRNA becomes negligible. In this scenario, we obtain that the presence of circRNA-miRNA interaction increases the amount of free mRNA, and, as a consequence, its translation for both the circuits reported in Fig. 5a,c. In fact, circRNA is capable to sequestrate miRNA molecules decreasing the amount of miRNA molecules capable to bind mRNA 3'UTR. note that in the complete circuit in Fig. 5c, the

presence of cirRNA increases the range of parameters for which there is multistability. Furthermore, the effect of circRNA on free mRNA increases with mRNA expression, thus increasing the distance between the solutions (Fig. 5d).

Since circRNA is expected to be more stable than its linear counterpart, in our model we can consider $\mu_C > \mu_T$. Thus, for a given range of transcription rates, mRNA can be in free state ($\mu < \mu_T$) while circRNA is bounded ($\mu > \mu_C$). This effect is even more evident when circRNA affinity for miRNA is higher than its linear counterpart (Fig. S1a). In this case, most of the cirRNA produced will be sequestrated by miRNA and will remain in a bound state (Fig.S1b), while the amount of free circRNA molecules would remain almost undetectable compared to free mRNA increase (Fig.S1a).

*Limiting reagent model.*A more complex relationship between circRNA production rate and mRNA level can be obtained under the hypothesis that circRNA production is due to the binding of the linear unspliced transcript with a protein or a complex of proteins (Q) that favour circularizaion and backsplicing. If the concentration of the protein Q is fixed when the transcription rate increases, the effective circRNA production rate could be expressed in terms of an Hill function: $Kc = \epsilon \frac{T}{T_Q + T}$, where ϵ depends on the concentration of Q and T_Q is related to T-Q binding affinity. For small transcription rates, ($T \ll T_Q$, Q abundant), the dependence of Kc on T is linear $K_C \approx \epsilon\, T/T_Q$, recovering the linear model presented in the previous section (Fig. 6a). However, increasing mRNA level ($T \gg T_Q$) the circRNA production rate becomes constant $K_C \approx \epsilon$. In this limit, the presence of miRNA-mediated crosstalk allows C_{eq} to increase more than linearly with T_{eq} while it C_{eq} becomes constant when miRNA contribute becomes negligible (Fig. 6b).

4 Discussion

EMT is a complex physiological process that can help cancer progression and metastasis, involving differential expression of many genes and noncoding RNAs [47,48,49,1]. The feedback loop between ZEB1 and the members of mir200 family, involving transcritional and post-transcriptional regulatory is the core of EMT regulatory network [41,23,24,25,49]. High ZEB1 expression in primary tumors and specific subpopulations of cells correlates with the presence of metastasis, drug resistance and poor prognosis [50,51,52,53,54].

In recent years, an increasing number of circRNAs have been recognized to play a role in the regulation of gene expression. One of the main mechanisms of action of circRNAs is the capability to bind miRNAs competing with their canonical targets [9,17,18,14]. Moreover, circRNAs have been found deregulated in different tumors and their altered expression seems to be related to tumor prognosis and aggressiveness [55,16,56,17,15,11,57, 58]. Recently, it has been shown that circZEB1 actively interacts with mir200a [59], but his specific role in the regulation of EMT was not investigated.

In this context, we have analyzed the level of expression of ZEB1 in human primary melanoma with respect to metastasis in public repositories (GDC database) and in two cell lines obtained from two distinct melanoma patients. Our results show that the level of expression of ZEB1 is consistently reduced in metastatic melanoma compared to their corresponding primary tumors. Interestingly, the same feature is observed in breast cancer, suggesting that it is a general feature of metastasis. The decreased expression level of mesenchymal markers in samples obtained from metastasic tumors appears to indicate that cells switch to an epithelial phenotype when they reach the metastatic site [50,53].

To better understand the role of circZEB1 in EMT, we investigated the ZEB1-circuit during the phenotypic switching of IgR39 melanoma cells. We recently demonstrated that IgR39 cells that are negative for CSCs markers are able to dynamically re-express the markers through a regulatory network that also involves EMT-related genes. Phenotypic switching does not happens gradually but through an overshoot in which cancer cells switch massively to the CSC phenotype. In this way, the tumor is able to regulate the number of CSCs in its bulk [6]. Accordingly, we found that the level of ZEB1 increases at the overshoot in IgR39 human melanoma cells, confirming their plastic expression of EMT markers [6]. However, we also found a constant a constant level of expression for circZEB1. To better understand the biological significance of the high level of circZEB1, we investigated with computational models two possible scenario: 1) a direct proportionality between the total transcription rate and the amount of circRNA produced (linear model); 2) the presence of a third factor that favors back-splicing (limiting reagent model). We investigated this second scenario because there are evidences of canonical spliceosome proteins playing an active role in circRNA biogenesis [60,61,62].

In the first scenario, the presence of ceRNA interaction between the species would predict a superlinear relationship between total free mRNA amount and circRNA amount [19], even in presence of transcriptional feedback loop. In the second scenario, at low transcription rates the direct proportionality between mRNA and and circRNA production rate is preserved and this model can not be distinguished from the first scenario. The fold change reduction of circZEB1 observed in metastatic cells (IgR37 and WM116) compared to the primary ones are thus coherent with both scenarios. On the other hand, at high transcription rate, the back-splicing

factor can become limiting and the two models diverge, predicting a constant level of circRNA at increasing mRNA expression. This corresponds very closely to our observations in IgR39 cells during phenotyping switching where the basal level of ZEB1 is high and increases even more at the overshoot. Hence, our model suggests that the regulation of circZEB1 depends by a back-splicing factor and that the constant level of circZEB1 during phenotypic switching can be explained by our model under the assumption of a high ZEB1 transcription rate.

All together, our findings show the possible use of circZEB1 as possible biomarker of aggressiveness in melanoma.

5 Acknowledgement

The project was supported by funded from the Center for Complexity and Biosystems of UniMI. The research leading to these results was funded by AIRC under IG2018-ID 21558 project-PI Putsch Michael.

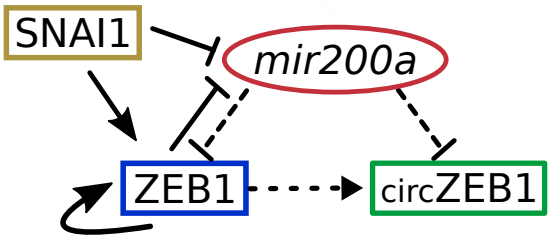

Fig. 1 ZEB1 circuit. The circuit is composed by a miRNA–TF mutually inhibiting loop involving transcritpional (solid lines) and post-transcriptional (dashed lines) regulation. A solid arrow denotes transcriptional activation, and a solid bar denotes transcriptional inhibition. Dashed arrow connecting ZEB1 to its circRNA indicates co-generation. SNAI1 is considered as an external signal regulating ZEB1 and mir200a at transcriptional level. ZEB1 self-activation is also included.

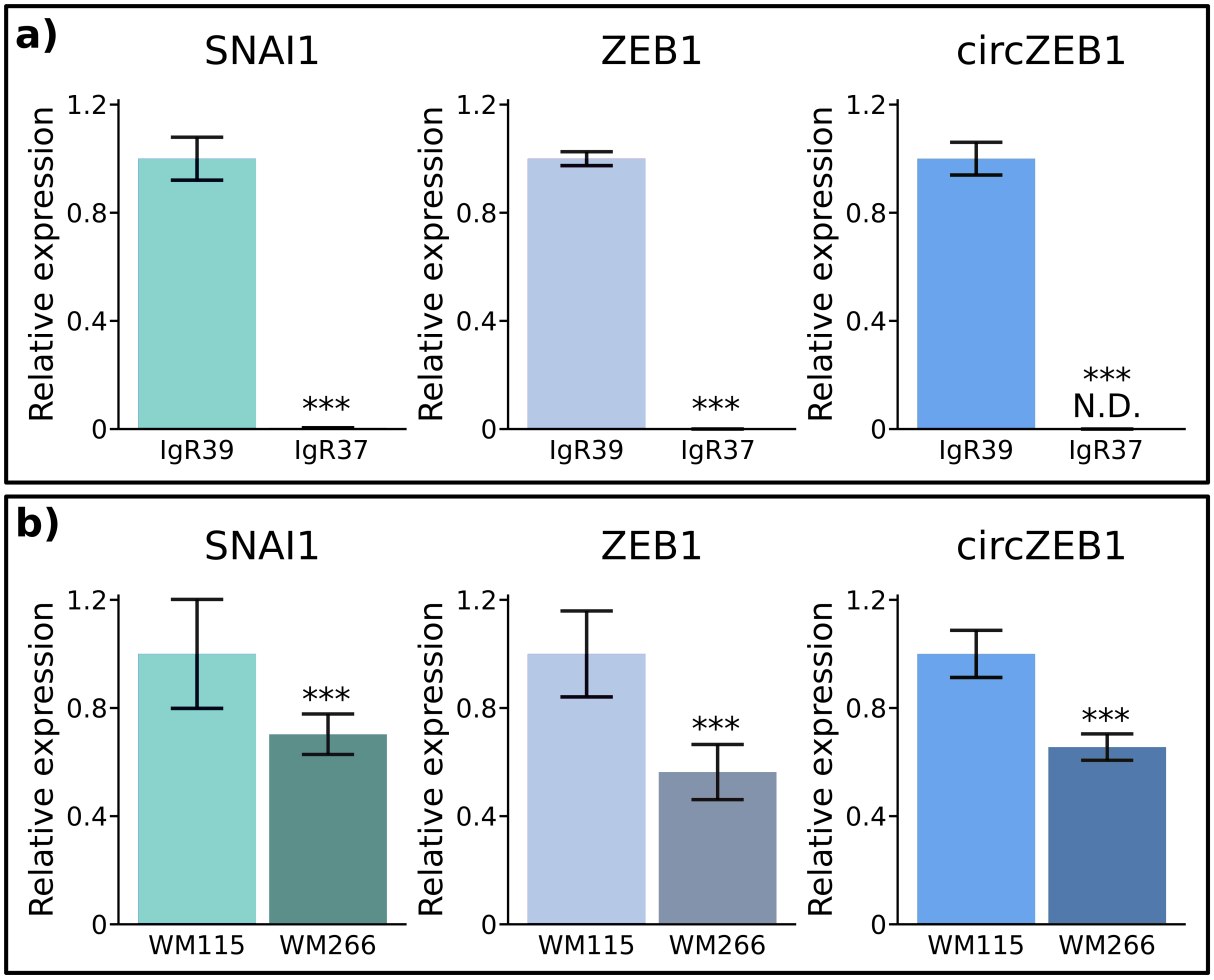

Fig. 2 Expression of ZEB1, SNAI1 and circZEB1 in primary and metastatic melanoma cell lines. qRT-PCR analysis of SNAI1, ZEB1 and circZEB1 expression was performed in primary (IgR39 and WM115) and corresponding metastatic (WM266 and IgR37) melanoma cell lines according to Materials and Methods section. T*** $p < 0.01$ versus primary tumor IgR39 or WM115 cells. The results are expressed as $2^{-\Delta Ct}$ using GAPDH as housekeeping gene.

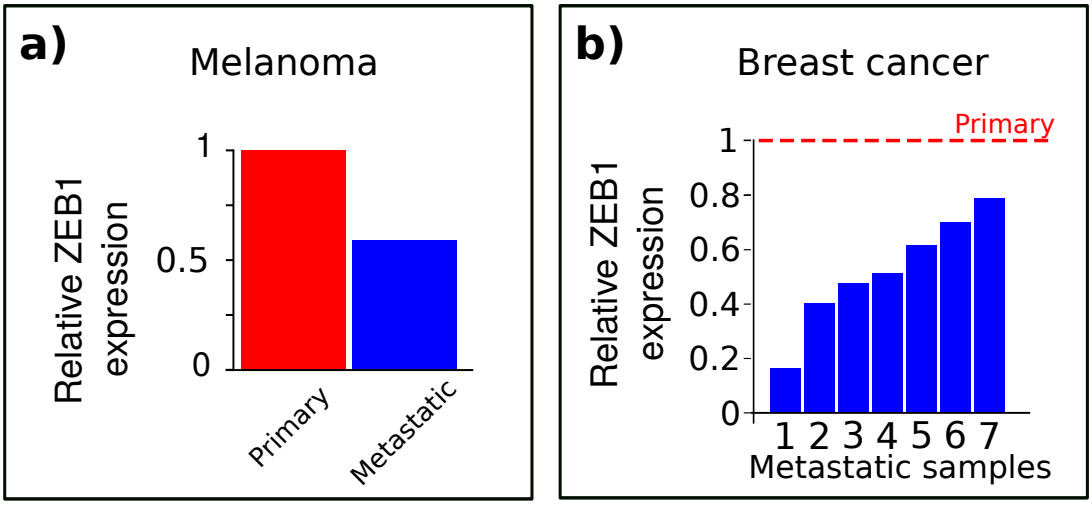

Fig. 3 ZEB1 mRNA expression in melanoma. (a) Plot shows the relative expression of ZEB1 in two paired primary (red) and metastatic (blue) melanoma samples from the same patient (TCGA-ER-A2NF) from GDC database. (b) Bar plot shows the relative expression of ZEB1 in seven metastatic breast cancer samples normalized over the corresponding primary tumors from the same patients. Dashed red line indicates the normalized level of ZEB1 in primary tumor samples. Fold changes are less than one in all the samples, showing that ZEB1 expression is reduced in metastatic tumors, coherently with what observed in melanoma. Data were downloaded from GDC database as described in materials and methods section. Correspondence between x-axis label and GDC cases: 1-TCGA-BH-A1ES, 2-TCGA-AC-A6IX, 3-TCGA-BH-A1FE, 4-TCGA-E2-A15K, 5-TCGA-E2-A15A, 6-TCGA-E2-A15E, 7-TCGA-BH-A18V.

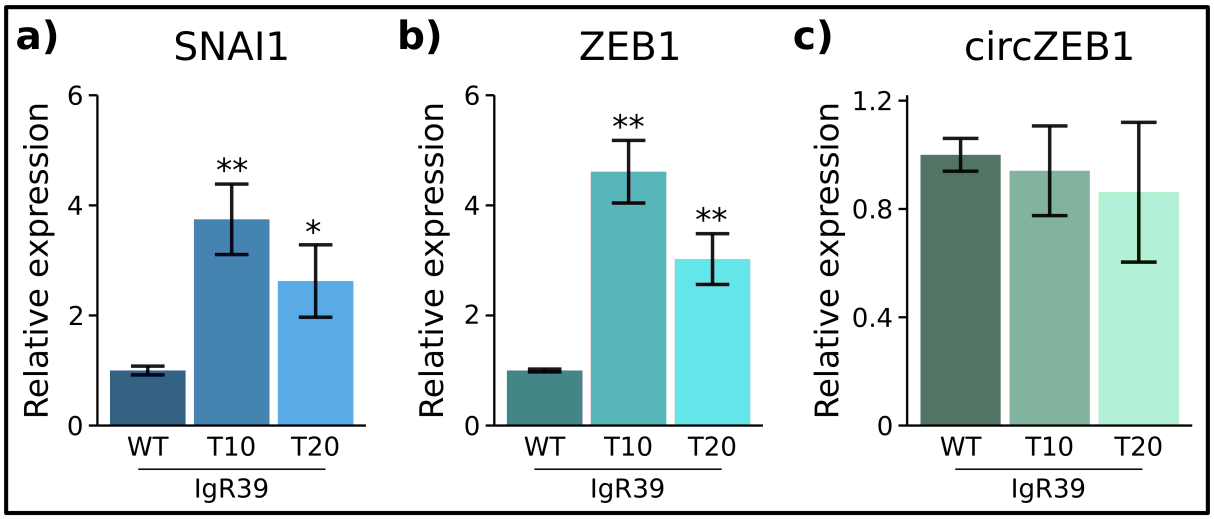

Fig. 4 Level of expression of ZEB1, SNAI1 and circZEB1 during phenotypic switching. qRT-PCR analysis of SNAI1 (a), ZEB1 (b) and circRNA (c) RNA levels was carried out on sorted IgR39 negative for CSC markers 10 days and 20 days after sorting as well as on IgR39 WT as described in Materials and Methods section. * p¡0.1, ** p¡0.05. The results are expressed as $2^{-\Delta Ct}$ using GAPDH as housekeeping gene.

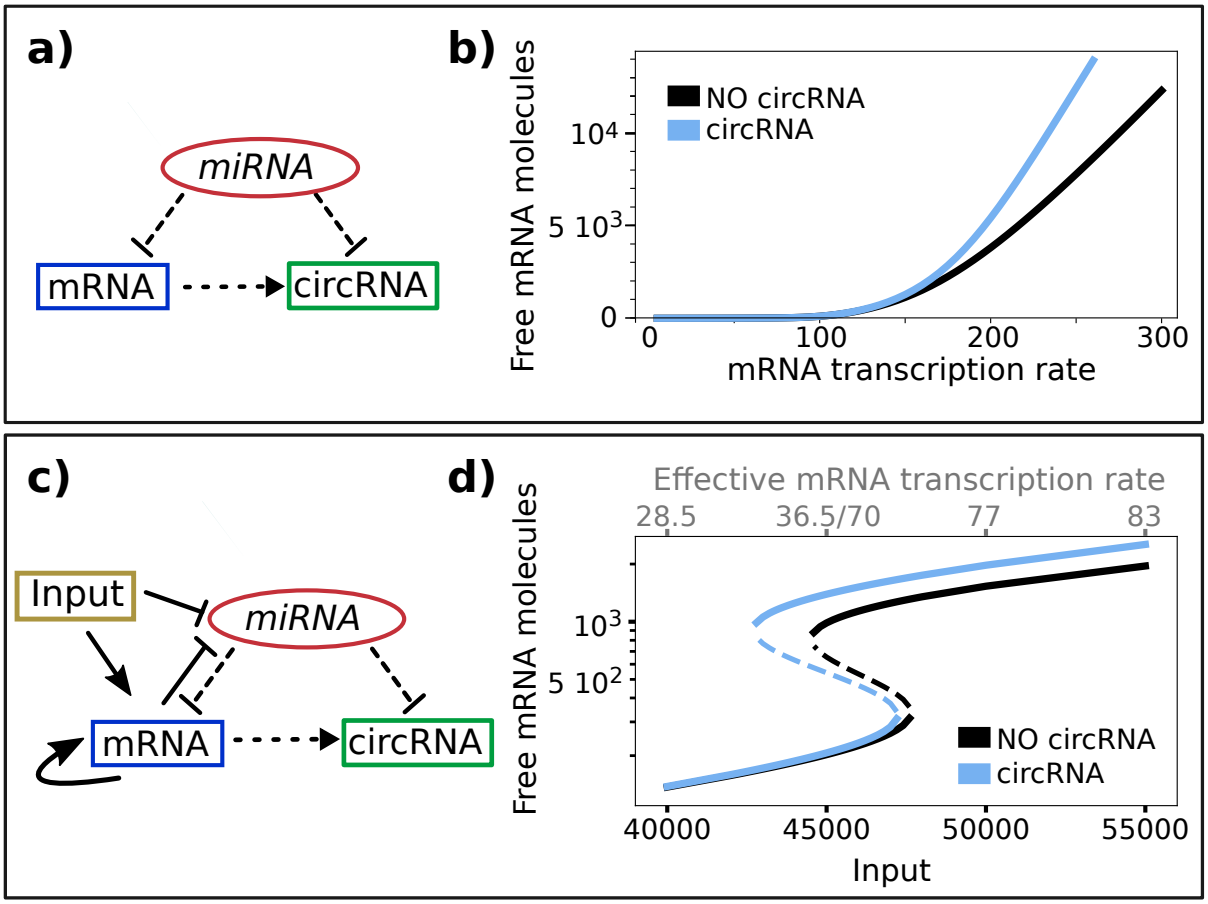

Fig. 5 Computational analysis of ZEB1—circuit Figure shows two schematic representation of miRNA mediated ceRNA circuits (a,c) and numerical prediction of mRNA concentration (b,d) in presence (light blue continuous line) and absence (black line) of the circRNA. a-b) Schematic representation of the miRNA-mediated ceRNA interaction network without mRNA autoactivation and miRNA transcriptional regulation. The model predicts an increase of free mRNA molecules in presence of circRNA as a function of mRNA transcription rate (panel b). c-d) Schematic representation of the miRNA-mediated ceRNA interaction network including mRNA autoactivation and miRNA transcriptional regulation and an external regulator (c). This model resembles the ZEB1-mir200-SNAI1 circuit reported in Fig.1. This kind of circuit can present multistability, as shown in panel (d). For the choosen set of parameters, the circuit presents two stable solutions (continuous lines) and one unstable state (dashed line) at fixed input rate (lower x axis). Total effective transcription rate is reported in the upper x-axis. The level of free mRNA increases in presence of co-generate circRNA for increasing transcription rate.

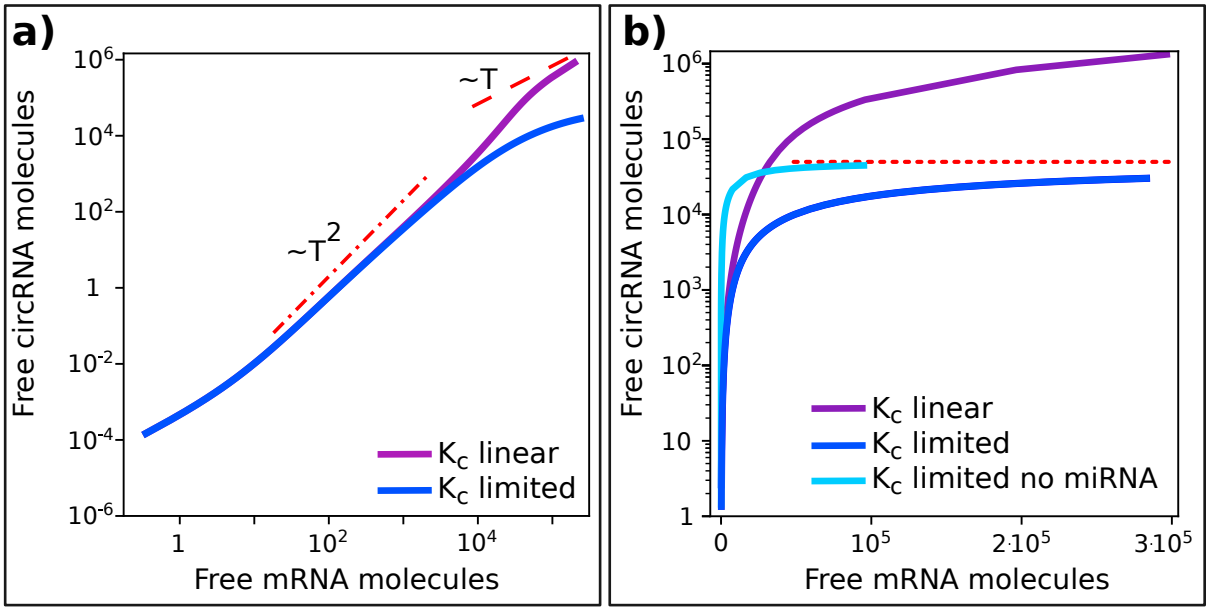

Fig. 6 CeRNA levels as a function of mRNA production rate. Figure shows the predicted level of free circRNA as a function of the linear transcript for the model presented in Figure 5a for two different functional forms of $K_C(T)$. (a) Linear dependency of circRNA production rate on T and Hill-like functional form (limiting reagent) are highly similar in a broad range of values of T (purple and blue lines respectively as in legend). For intermediate values of T both the models give an increase of C that is slightly less than quadratic (dashed-dotted red line) while for large T the two models diverge: the first model increases linearly (red dashed line), while limiting-reagent model shows a sublinear growth of C. (b) Same data as in panel (a) are plotted in semi-log scale. It is evident that limiting reagent model (blue continuous line) tend to a threshold value (dotted red line), while C increases continuously in linear model (continuous purple line). Note that the behavior of C at intermediate transcription rates is determined by the presence of miRNA. In fact, absence of miRNA implies a faster increase of C towards its limit value (light blue continuous line). All the parameters are maintained constant in the two models, decay rate of T is rescaled in order to make the models comparable. In the limiting model K_C has been chosen in order to have $\epsilon_{lim}/T_Q = \epsilon_{linear}$ ensuring that C production rate at low T is identical in the two models.

References

1. C.A.M. La Porta, S. Zapperi, Semin Cancer Biol **53**, 42 (2018). DOI 10.1016/j.semcancer.2018.07.003
2. C.A.M. La Porta, S. Zapperi, Semin Cancer Biol **44**, 3 (2017). DOI 10.1016/j.semcancer.2017.02.007
3. A. Kreso, C.A. O'Brien, P. van Galen, O.I. Gan, F. Notta, A.M.K. Brown, K. Ng, J. Ma, E. Wienholds, C. Dunant, A. Pollett, S. Gallinger, J. McPherson, C.G. Mullighan, D. Shibata, J.E. Dick, Science **339**(6119), 543 (2013). DOI 10.1126/science.1227670
4. S.V. Sharma, D.Y. Lee, B. Li, M.P. Quinlan, F. Takahashi, S. Maheswaran, U. McDermott, N. Azizian, L. Zou, M.A. Fischbach, K.K. Wong, K. Brandstetter, B. Wittner, S. Ramaswamy, M. Classon, J. Settleman, Cell **141**(1), 69 (2010). DOI 10.1016/j.cell.2010.02.027
5. H. Easwaran, H.C. Tsai, S.B. Baylin, Mol Cell **54**(5), 716 (2014). DOI 10.1016/j.molcel.2014.05.015
6. A.L. Sellerio, E. Ciusani, N.B. Ben-Moshe, S. Coco, A. Piccinini, C.R. Myers, J.P. Sethna, C. Giampietro, S. Zapperi, C.A.M. La Porta, Sci Rep **5**, 15464 (2015). DOI 10.1038/srep15464
7. J. Jia Chan, Y. Tay, International Journal of Molecular Sciences **19**, 1310 (2018). DOI 10.3390/ijms19051310
8. L.L. Chen, Nature Reviews Molecular Cell Biology **17**(4), 205 (2016). DOI 10.1038/nrm.2015.32. Cited By 18
9. S. Memczak, M. Jens, A. Elefsinioti, F. Torti, J. Krueger, A. Rybak, L. Maier, S.D. Mackowiak, L.H. Gregersen, M. Munschauer, et al., Nature **495**(7441), 333 (2013)
10. W.R. Jeck, J.A. Sorrentino, K. Wang, M.K. Slevin, C.E. Burd, J. Liu, W.F. Marzluff, N.E. Sharpless, Rna **19**(2), 141 (2013)
11. T.B. Hansen, J. Kjems, C.K. Damgaard, Cancer research **73**(18), 5609 (2013)
12. Y. li, Q. Zheng, C. Bao, S. Li, W. Guo, J. Zhao, C. Di, J. Gu, X. He, S. Huang, Cell research **25** (2015). DOI 10.1038/cr.2015.82
13. S. Memczak, P. Papavasileiou, O. Peters, N. Rajewsky, PloS one **10**(10), e0141214 (2015)
14. S. Huang, B. Yang, B. Chen, N. Bliim, U. Ueberham, T. Arendt, M. Janitz, Genomics **109**(5-6), 401 (2017)
15. J. Chen, Y. Li, Q. Zheng, C. Bao, J. He, B. Chen, D. Lyu, B. Zheng, Y. Xu, Z. Long, et al., Cancer letters **388**, 208 (2017)
16. P. Li, S. Chen, H. Chen, X. Mo, T. Li, Y. Shao, B. Xiao, J. Guo, Clinica chimica acta **444**, 132 (2015)
17. H. Xie, X. Ren, S. Xin, X. Lan, G. Lu, Y. Lin, S. Yang, Z. Zeng, W. Liao, Y.Q. Ding, et al., Oncotarget **7**(18), 26680 (2016)
18. Q. Zheng, C. Bao, W. Guo, S. Li, J. Chen, B. Chen, Y. Luo, D. Lyu, Y. Li, G. Shi, L. Liang, J. Gu, X. He, S. Huang, Nature Communications **7** (2016). DOI 10.1038/ncomms11215
19. M.R. Fumagalli, S. Zapperi, C.A. La Porta, Journal of theoretical biology **454**, 386 (2018)
20. L. Salmena, L. Poliseno, Y. Tay, L. Kats, P. Paolo Pandolfi, Cell **146**, 353 (2011). DOI 10.1016/j.cell.2011.07.014
21. C. Bosia, A. Pagnani, R. Zecchina, PLoS ONE **8**(6), 1 (2013)
22. M. Figliuzzi, E. Marinari, A. De Martino, Biophysical journal **104**, 1203 (2013). DOI 10.1016/j.bpj.2013.01.012
23. S.M. Park, A. B Gaur, E. Lengyel, M. E Peter, Genes & development **22**, 894 (2008). DOI 10.1101/gad.1640608
24. U. Burk, J. Schubert, U. Wellner, O. Schmalhofer, E. Vincan, S. Spaderna, T. Brabletz, EMBO Reports **9**(6), 582 (2008). DOI 10.1038/embor.2008.74
25. G. Wang, X. Guo, W. Hong, Q. Liu, T. Wei, C. Lu, L. Gao, D. Ye, Y. Zhou, J. Chen, J. Wang, M. Wu, H. Liu, J. Kang, Proceedings of the National Academy of Sciences of the United States of America **110**(8), 2858 (2013). DOI 10.1073/pnas.1212769110
26. T.U. Consortium, Nucleic Acids Research **43**, D204 (2015). URL `http://www.uniprot.org`
27. D. R Zerbino, P. Achuthan, W. Akanni, M. Ridwan Amode, D. Barrell, J. Bhai, K. Billis, C. Cummins, A. Gall, C. García Girón, L. Gil, L. Gordon, L. Haggerty, E. Haskell, T. Hourlier, O. G Izuogu, S. H Janacek, T. Juettemann, J. Kiang To, P. Flicek, Nucleic acids research **46** (2017). DOI 10.1093/nar/gkx1098
28. Y.C. Liu, J. Li, C.H. Sun, E. Andrews, R.F. Chao, F.M. Lin, S.L. Weng, S.D. Hsu, C.C. Huang, C. Cheng, C.C. Liu, H.D. Huang, Nucleic acids research **44** (2015). DOI 10.1093/nar/gkv940
29. P. Glažar, P. Papavasileiou, N. Rajewsky, RNA (New York, N.Y.) **20** (2014). DOI 10.1261/rna.043687.113
30. Y. Lu, J. Lu, X. Li, H. Zhu, X. Fan, S. Zhu, Y. Wang, Q. Guo, L. Wang, Y. Huang, M. Zhu, Z. Wang, BMC Cancer **14**(1), 85 (2014). DOI 10.1186/1471-2407-14-85. URL `https://doi.org/10.1186/1471-2407-14-85`
31. D. Iliopoulos, C. Polytarchou, M. Hatziapostolou, F. Kottakis, I. Maroulakou, K. Struhl, P. Tsichlis, Science signaling **2**, ra62 (2009). DOI 10.1126/scisignal.2000356
32. M. Pichler, A. Ress, E. Winter, V. Stiegelbauer, M. Karbiener, D. Schwarzenbacher, M. Scheideler, C. Ivan, S. W Jahn, T. Kiesslich, A. Gerger, T. Bauernhofer, G. Calin, G. Hoefler, British journal of cancer **110** (2014). DOI 10.1038/bjc.2014.51
33. T. Guan, C.X. Dominguez, R.A. Amezquita, B.J. Laidlaw, J. Cheng, J. Henao-Mejia, A. Williams, R.A. Flavell, J. Lu, S.M. Kaech, Journal of Experimental Medicine **215**(4), 1153 (2018). DOI 10.1084/jem.20171352. URL `http://jem.rupress.org/content/215/4/1153`
34. F. Facchetti, S. Previdi, M. Ballarini, S. Minucci, P. Perego, C. Porta, Apoptosis **9**(5), 573 (2004). DOI 10.1023/B:APPT.0000038036.31271.50
35. A. Untergasser, I. Cutcutache, T. Koressaar, J. Ye, B. C Faircloth, M. Remm, S. G Rozen, Nucleic acids research **40**, e115 (2012). DOI 10.1093/nar/gks596
36. C. Camacho, G. Coulouris, V. Avagyan, N. Ma, J. Papadopoulos, K. Bealer, T. Madden, BMC Bioinformatics **10**(421) (2009). DOI 10.1186/1471-2105-10-421.
37. R Core Team, *R: A Language and Environment for Statistical Computing*. R Foundation for Statistical Computing, Vienna, Austria (2015). URL `https://www.R-project.org/`
38. R. Grossman, A. P. Heath, V. Ferretti, H. E. Varmus, D. R. Lowy, W. A. Kibbe, L. M. Staudt, New England Journal of Medicine **375**, 1109 (2016). DOI 10.1056/NEJMp1607591
39. S. Brabletz, T. Brabletz, EMBO reports **11**, 670 (2010). DOI 10.1038/embor.2010.117
40. M. Lu, M.K. Jolly, H. Levine, J.N. Onuchic, E. Ben-Jacob, Proceedings of the National Academy of Sciences **110**(45), 18144 (2013)
41. M. Lu, M.K. Jolly, R. Gomoto, B. Huang, J. Nelson Onuchic, E. Ben-Jacob, The journal of physical chemistry. B **117** (2013). DOI 10.1021/jp403156m
42. S. Bail, M. Swerdel, H. Liu, X. Jiao, L.A. Goff, R.P. Hart, M. Kiledjian, Rna **16**(5), 1032 (2010)
43. S. Rüegger, H. Großhans, Trends in biochemical sciences **37**(10), 436 (2012)
44. Z. Zhang, Y.W. Qin, G. Brewer, Q. Jing, Wiley Interdisciplinary Reviews: RNA **3**(4), 593 (2012)
45. A. Martirosyan, A. De Martino, A. Pagnani, E. Marinari, Scientific Reports **7** (2017). DOI 10.1038/srep43673
46. J.D. Hunter, Computing In Science & Engineering **9**(3), 90 (2007). DOI 10.1109/MCSE.2007.55
47. R. Kalluri, R. Weinberg, The Journal of clinical investigation **119**, 1420 (2009). DOI 10.1172/JCI39104
48. F. Font-Clos, S. Zapperi, C.A. La Porta, Proceedings of the National Academy of Sciences **115**(23), 5902 (2018)
49. M.K. Jolly, M. Boareto, B. Huang, D. Jia, M. Lu, E. Ben-Jacob, J. N Onuchic, H. Levine, Frontiers in Oncology (2015). DOI 10.3389/fonc.2015.00155

50. H. Kurahara, S. Takao, K. Maemura, Y. Mataki, T. Kuwahata, K. Maeda, Q. Ding, M. Sakoda, S. Iino, S. Ishigami, et al., Journal of surgical oncology **105**(7), 655 (2012)
51. G. Richard, S. Dalle, M.A. Monet, M. Ligier, A. Boespflug, R.M. Pommier, A. de la Fouchardière, M. Perier-Muzet, L. Depaepe, R. Barnault, et al., EMBO molecular medicine **8**(10), 1143 (2016)
52. J. Sakata, F. Utsumi, S. Suzuki, K. Niimi, E. Yamamoto, K. Shibata, T. Senga, F. Kikkawa, H. Kajiyama, Oncotarget **8**(59), 99482 (2017)
53. C. Kahlert, S. Lahes, P. Radhakrishnan, S. Dutta, C. Mogler, E. Herpel, K. Brand, G. Steinert, M. Schneider, M. Mollenhauer, et al., Clinical cancer research **17**(24), 7654 (2011)
54. A. Eger, K. Aigner, S. Sonderegger, B. Dampier, S. Oehler, M. Schreiber, G. Berx, A. Cano, H. Beug, R. Foisner, Oncogene **24**(14), 2375 (2005)
55. L. Kristensen, T. Hansen, M. Venø, J. Kjems, Oncogene **37**(5), 555 (2018)
56. X. Shang, G. Li, H. Liu, T. Li, J. Liu, Q. Zhao, C. Wang, Medicine **95**(22) (2016)
57. M. Sand, F.G. Bechara, T. Gambichler, D. Sand, M. Bromba, S.A. Hahn, E. Stockfleth, S. Hessam, Journal of dermatological science **83**(3), 210 (2016)
58. L.h. Jiang, D.w. Sun, J.c. Hou, Z.l. Ji, et al., Breast Cancer **25**(1), 1 (2018)
59. Y. Gong, et al., Cancer cell international **18**(1), 116 (2018)
60. S. Starke, I. Jost, O. Rossbach, T. Schneider, S. Schreiner, L.H. Hung, A. Bindereif, Cell reports **10**(1), 103 (2015)
61. S.J. Conn, K.A. Pillman, J. Toubia, V.M. Conn, M. Salmanidis, C.A. Phillips, S. Roslan, A.W. Schreiber, P.A. Gregory, G.J. Goodall, Cell **160**(6), 1125 (2015)
62. L.L. Chen, L. Yang, RNA biology **12**(4), 381 (2015)
63. L. Hill, G. Browne, E. Tulchinsky, International journal of cancer. Journal international du cancer **132** (2013). DOI 10.1002/ijc.27708

Supplementary Information

Parameters selection

ZEB1 has two binding sites on mir200b-mir200a-mir429 cluster promoter, shared with ZEB2 and SNAI1[39], and has multiple E-box binding sites on its own promoter, promoting its self-activation through stabilization of SMAD complexes [63]. We model two distinct binding site of for SNAI1 and ZEB1 on both mir200 and ZEB1 and we suppose them to be independent.

Model description

Here we present in detail our model for ZEB1-mir200 ceRNA circuit and a more generalized framework for modeling mirRNA-mediated ceRNA circuit including multiple TFs and miRNAs binding sites.

We recall that, for sake of simplicity, we assume that the cross talk and relevant changes in species abundances is restricted to the circuit reported in Fig.1 involving a single miRNA and two RNAs targets with an external tanscriptional activator, treating the contributions of other species as a constant and implicitly including them into the decay rates.

TFs binding on gene promoter

In this section we will derive the occupation probability and total transcription rate for mir200 and ZEB1 promoter under the hypothesis of two non-competitive and binding sites for ZEB1 ans SNAI1 proteins.

In general, a promoter D with a single binding site can be in the free state or occupied (D^*) by its transcription factor (TF). We associate to the transcription factor A binding/unbinding rates ξ_A and δ_A.

At equilibrium, the probability that the promoter exist in free ($[D]$) or bound ($[D*]$) state are coupled by

$$[D^*] = \frac{\xi_D}{\delta_D}\,[A]^{n_A}\,[D] = \left(\frac{[A]}{[A_0]}\right)^{n_A}[D] \tag{2}$$

where n_A indicate the transcription factor cooperativity.

Imposing normalization condition $[D] + [D^*] = 1$ we obtain that $[D]$ and $[D^*]$ have the functional form of activating and inhibitory Hills functions

$$\begin{cases} [D] &= \dfrac{1}{1+([A]/[A_0])^{n_A}} = H^-(A, n_A) \\ [D^*] &= \dfrac{([A]/[A_0])^{n_A}}{1+([A]/[A_0])^{n_A}} = H^+(A, n_A) \end{cases} \tag{3}$$

In our model we consider two distinct binding site for SNAI1 and ZEB1 on both mir200 and ZEB1, so that the promoter can be free, bounded by either ZEB1 or SNAI1 or in the two-TF-bounded form. Thus, states of the promoter can be expressed in terms of Hills functions for a single binding site for either ZEB1 or SNAI1 (see also [41]), and the two binding sites are coupled by normalization condition $[D]+[D^S]+[D^Z]+[D^{SZ}] = 1$.

Note that, in general, the total effective transcription rate can be calculated as $\kappa_{tot} = \sum_{i=0,n} \kappa^{i*}\binom{n}{i}[D^{i*}]$ where κ^{i*} is the transcription rate associated with state $[D^{i*}]$. Thus, it is immediate to obtain that the total transcription rate is given by

$$\begin{aligned} \kappa(S,Z) = k0 \quad & H^-(S,n_S)H^-(Z,n_Z) \\ +k1_S \quad & H^+(S,n_S)H^-(Z,n_Z) + k1_Z\, H^-(S,n_S)H^+(Z,n_Z) \\ +k2 \quad & H^+(S,n_S)H^+(Z,n_Z) \end{aligned} \tag{4}$$

For sake of simplicity, we consider $n_S = n_Z = 2$ for both mir200a and ZEB1. While a different choice of cooperative parameters would change the output of the model and the multistability region and the number of stable solution, it does not influence the general results obtained and the global effect of the presence of circRNA.

For mir200a the TFs act as inhibitors, and as a consequence $k0 > k1_S, k1_Z > k2$, while for ZEB1 $k0 < k1_S, k1_Z < k2$.

General model for ceRNA circuit

In the following we present in detail our model for miRNA mediated ceRNA circuit for a generic mRNA/circRNA couple.

MiRNA-mediated interactions are modeled using a set of differential equation in agreement with our previous work []. This model include miRNA molecules (μ), the target RNAs (T, mRNA and C, circRNA) and the corresponding miRNA-target complexes as well as an external transcription factors S and protein P produced by T.

In principle, we should define $T'_{n,\alpha}$ as the number of mRNA molecules with n miRNA bound in a specific configuration α among all the possible $\binom{M}{n}$. Thus, the total number of mRNA molecules bound by α miRNA is $T_n = \sum_n T'_{n,\alpha}$.

For each single configuration, we indicate with ξ'_{T_n} the rate of binding of a single miRNA to an mRNA molecule with $n-1$ binding sites already occupied and δ'_{T_n} is the unbinding rate of one single miRNA molecule from an mRNA with n miRNAs. These parameters can be referred to the total number of mRNA bind to n miRNA T_n using a rescaling to account for the multiplicity of the configurations. The global parameters result $\xi_{T_n} = (M-1+n)\xi'_{T_n}$ and $\delta_{T_n} = n\delta'_{T_n}$, while the decay rate is not affected by rescaling ($\gamma_n = \gamma'_n$). In the following we will consider the global parameters including the correct multiplicity and use C_1 to indicate the circRNA-miRNA complex and T_1, T_2 for mRNA with one-miRNA and two miRNA bound respectively according to ZEB1 3'UTR mir200a binding sites[39,25]. Moreover, considering multiple miRNA binding/unbinding events occurring at the same time does not affects our reasoning, and this additional layer of complexity can be adsorbed by parameter rescaling.

The general model illustrated in Fig. 1 and Fig. 4 can be described with the following kinetics equations

$$
\begin{aligned}
\frac{d\mu}{dt} &= \kappa_\mu - \gamma_\mu \mu - \xi_{T_1}\mu T - \xi_{C_1}\mu C + \delta_{T_1}T_1 + \gamma_{T_1}\beta_{T_1}T_1 + \delta_{T_2}T_2 + 2\gamma_{T_2}\beta_{T_2}T_2 + \delta_{C_1}C_1 + \gamma_{C_1}\beta_{Cs}C_1 \\
\frac{dT}{dt} &= \kappa_T - \gamma_T T - K_C(\epsilon, T) - \xi_{T_1}T\mu + \delta_{T_1}T_1 \\
\frac{dC}{dt} &= K_C(\epsilon, T) - \gamma_C C - \xi_{C_1}C\mu + \delta_{C_1}C_1 \\
\frac{dT_1}{dt} &= -\gamma_{T_1}T_1 + \xi_{T_1}T\mu - \delta_{T_1}T_1 - \xi_{T_2}T_2\mu + \delta_{T_2}T_2 \\
\frac{dT_2}{dt} &= -\gamma_{T_2}T_2 + \xi_{T_2}T\mu - \delta_{T_2}T_2 \\
\frac{dC_1}{dt} &= -\gamma_{C_1}C_1 + \xi_{C_1}C\mu - \delta_{C_1}C_1 \\
\frac{dP}{dt} &= -\gamma_P P + L(\mu)T
\end{aligned}
\tag{5}
$$

where κ and γ are the synthesis and decay rates, ξ_{A_s} are the association rate between miRNA and the specie A to create the complex A_s and δ_{A_s} is the corresponding dissociation rate. The parameter β gives the probability that the miRNA molecule is recycled after the decay of the complex miRNA-target and $L(\mu)$ it the total translation rate. Note that the total translation rate $L(\mu)$ depends on the number of the miRNA that are attached to mRNA and we choose explicitly model each binding site contribution, in contrast to previous works []. A general formulation of the multiple binding sites model is reported in the subsection [].

Note that, according to previous section the synthesis rate κ_μ and κ_T can be expressed as Hills functions of TFs inshibitors/activator.

Considering the system in Eq.(5) and imposing the steady state conditions, it is straightforward to obtain implicit solutions for the free species

$$
\begin{aligned}
\mu_{eq} &= \frac{\kappa_\mu}{\gamma_\mu + G_T(\mu, M_T)T_{eq} + G_C(\mu, M_C)C_{eq})} \\
T_{eq} &= \frac{\kappa_T}{\gamma_T(1 + \mu_{eq}/\mu_T)} \\
C_{eq} &= \frac{\kappa_C}{\gamma_C(1 + \mu_{eq}/\mu_C)}
\end{aligned}
\tag{6}
$$

where we have introduced the rescaled parameters

$$\mu_T = \gamma_T / \left(\xi_T F_T(\mu, M_T)\right) \mu_C = \gamma_C / \left(\xi_C F_C(\mu, M_C)\right) \tag{7}$$

and $F(\mu, M)$, $G(\mu, M)$ are functions that depend on the total number of miRNA binding sites M and account for the contribution of all the bounded species. An explicit and general expression for $F(\mu, M)$ is presented in the next section.

The implicit equilibrium solution give in Eq.(6) could lead in principle to multiple positive solutions in function of the cooperativity of the Hill functions κ_μ and κ_T. When we can consider the production rates as constant, there is only one real positive solution for the concentration of RNA species.

Note that the parameter β is essential for ceRNA crosstalk, since for $\beta = 1$ (perfectly catalytic interaction) $\widetilde{\xi_{A1i}} = 0$ and, as a consequence, the concentration of miRNA is not influenced by its targets.

Multiple miRNA binding sites

In this section we will consider the general case of a mRNA having M equivalent non cooperative miRNA binding sites. Using the notation introduced in previous section, the complete system is given by

$$\begin{aligned}
\frac{d\mu}{dt} &= \kappa_\mu - \gamma_\mu \mu - \textstyle\sum_{n=1,M} \xi_n \mu T_{n-1} + \sum_{n=1,M} \delta_n T_n + \sum_{n=1,M} n\gamma_n \beta T_n \\
\frac{dT}{dt} &= \kappa_T - \gamma_T T - \xi_{T_1} T\mu + \delta_{T_1} T_1 \\
\frac{dT_1}{dt} &= -\gamma_{T_1} T_1 + \xi_{T_1} T\mu - \delta_{T_1} T_1 - \xi_{T_2} T_1 \mu + \delta_{T_2} T_2 \\
&\ldots \\
\frac{dT_{M-1}}{dt} &= -\gamma_{T_{M-1}} T_{M-1} + \xi_{T_{M-1}} T_{M-2}\mu - \delta_{T_{M-1}} T_{M-1} - \xi_{T_M} T_{M-1}\mu + \delta_{T_M} T_M \\
\frac{dT_M}{dt} &= -\gamma_{T_M} T_M + \xi_{T_M} T_{M-1}\mu - \delta_{T_M} T_M
\end{aligned} \tag{8}$$

Imposing steady state condition, it is possible to solve recursively the equations

$$\begin{aligned}
T_M &= \frac{\xi_{T_M}}{\gamma_{T_M} + \delta_{T_M}} \mu T_{M-1} \\
T_{M-1} &= \frac{\xi_{T_{M-1}}}{\gamma_{T_{M-1}} + \delta_{T_{M-1}} + \xi_{T_M}\mu \left(1 - \dfrac{\delta_{T_M}}{\gamma_{T_M} + \delta_{T_M}}\right)} \mu T_{M-2} \\
&\ldots
\end{aligned} \tag{9}$$

and in general

$$T_n = \frac{\xi_{T_n}}{\gamma_{T_n} + \delta_{T_n} + \xi_{T_{n+1}}\mu \left(1 - \delta_{T_{n+1}} f_M(n+1, \mu)\right)} \mu T_{n-1} \tag{10}$$

where we introduced the function

$$f_M(n, \mu) = \frac{1}{\gamma_{T_n} + \delta_{T_n} + \xi_{T_{n+1}}\mu \left(1 - \delta_{T_{n+1}} f_M(n+1, \mu)\right)} \tag{11}$$

for $n = 1, M-1$ and

$$f_M(M, \mu) = \frac{1}{\gamma_{T_M} + \delta_{T_M}} \tag{12}$$

Note that given $\delta_{T_M} f_M(M, \mu) < 1$, we obtain that $\delta_{T_n} f_M(n, \mu) < 1$ $\forall n$ and $f_M(n, \mu)$ is always positive. In the limit of very small μ (i.e. $\mu << \mu_{T_n}$), $f_M(n, \mu) \approx 1/(\delta + \gamma)$ while for very large μ, $f_M(n, \mu) \to 0$

In conclusion, all the steady state solution for $T_M..T_1$ can be adsorbed in a factor $F(\mu, M) = (1 - \delta_{T_1} f_M(1, \mu))$, $\gamma_{T_1}/(\delta_{T_1} + \gamma_{T_1}) < F(\mu, M) < 1$.

It can be useful to derive all the species as a function of T_0

$$\begin{aligned}
T_n &= \xi_{T_n} f_M(n, \mu) \mu\, T_{n-1} \\
&= \textstyle\prod_{m=n,1} \left(\xi_{T_m} f_M(m, \mu)\mu\right) T
\end{aligned} \tag{13}$$

in the limit of very small μ, only $n = 1$ gives a contribute while for very large μ all the terms give a contribute, that is $\propto 1/(1 - \delta * f)$

and the reduced system is

$$\begin{aligned} \frac{d\mu}{dt} &= \kappa_\mu - \gamma_\mu \mu + \textstyle\sum_{n=1,M} \left((\delta_{T_n} + n\gamma_{T_n}\beta) f_M(n,\mu) - 1 \right) \xi_{T_n} \mu \, T_{n-1} \\ \frac{dT}{dt} &= \kappa_T - \gamma_T T - \xi_{T_1} F(\mu, M) T \mu \end{aligned} \tag{14}$$

In general, when considering the production of a protein P, we have to consider the total translation rate L as the sum the of translation rates $l_{P,n}$ of T_n

$$\begin{aligned} \frac{dP}{dt} &= l_{P,0} T + \kappa_{P,1} T_1 + ... - \gamma_P P \\ &= \textstyle\sum \kappa_{P,n} \prod_{m=n,1} \left(\xi_{T_m} f(m,\mu) \mu \right) T - \gamma_P P \\ &= L(\mu) T - \gamma_P P \end{aligned} \tag{15}$$

Supplementary figures

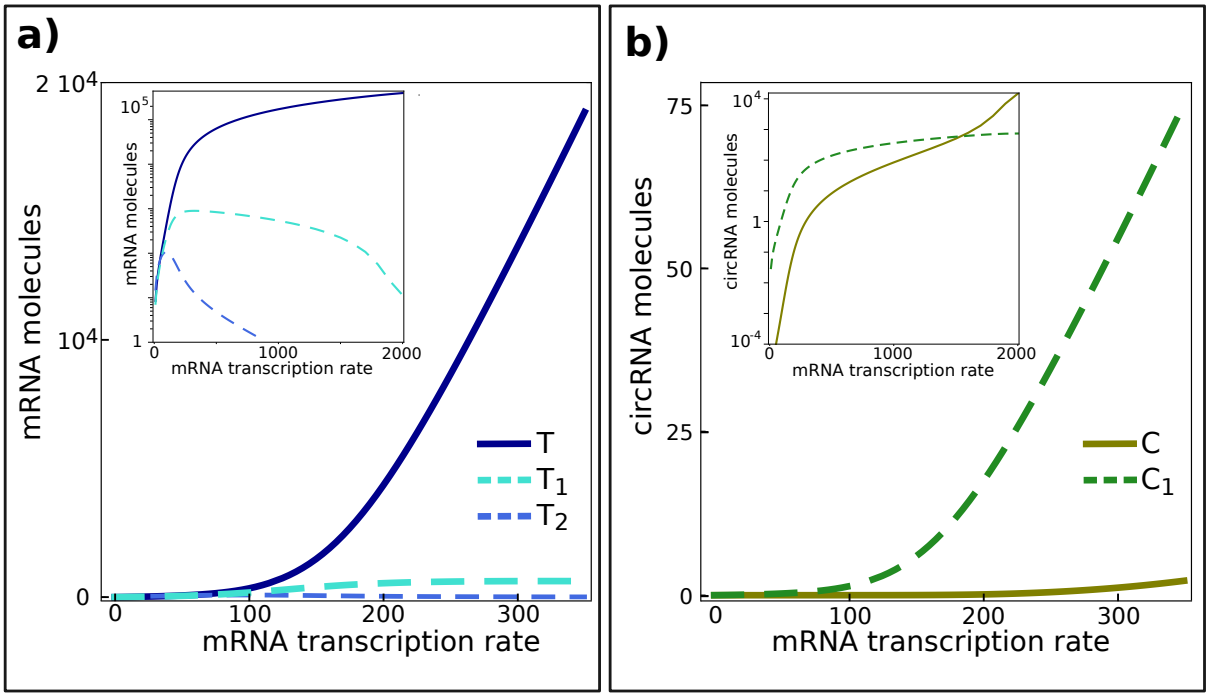

Fig. S1 CeRNAs levels as a function of mRNA production rate. Figure shows the predicted level of free mRNA and circRNA (T and C) as well as the amount of molecules bound by one (T_1, C_1) or two (T_2) miRNA molecules according to model in Fig.1 when circRNA/miRNA affinity is larger than mRNA/miRNA affinity. For small values of mRNA transcription rate the bound forms (dashed lines) are much more abundant than free RNAs (continuous lines).Insets shows model solution at larger mRNA transcription rate. When transcription rate increases, fre mRNA becomes more abundant that bounded forms (a), while free circRNA C remains low compared to $C1$ because $\mu_C >> \mu_T$. Further increase of mRNA transcription rate leads to a decrease of miRNA molecules (not shown) and the system approach free state. The threshold transcription rate at which the cross from bounded to unbounded state is observed depends on the relative ceRNA/miRNA affinity.